*Article*

# Thin Luminous Tracks of Particles from Electrodes with a Small Radius of Curvature in Pulsed Nanosecond Discharges in Air and Argon

**Victor F. Tarasenko[1*], Dmitry V. Beloplotov[1], Alexei N. Panchenko[1], and Dmitry A. Sorokin[1]**

1; Laboratory of Optical Radiation, Institute of High Current Electronics, Siberian Branch (SB), Russian Academy of Sciences, Akademicheskii Av. 2/3, Tomsk, 634055, Russia

* Correspondence: vft@loi.hcei.tsc.ru; Tel.: (+73822491385)

**Abstract:** Features of nanosecond discharge development in a non-uniform electric field are studied experimentally. High spatial resolution imaging showed that thin luminous tracks of great length with a cross-section of a few microns are observed against the background of discharge glow in air and argon. It has been established that the detected tracks are adjacent to brightly luminous white spots on the electrodes or to the vicinity of these spots, and are associated with the flight of small particles. It is shown that the traces have various shapes and change from pulse to pulse. The particle tracks may look like curvy or straight lines. In some photos, they can change the direction of movement to the opposite. The particle trace was found to abruptly cut off and a bright flash is visible at the trail break point. The color of the tracks differs from that of the spark leaders, while the bands of the second positive nitrogen system dominate in the gap spectra during the existence of a diffuse discharge. Areas of blue light are evident near the electrodes, as well. Development of glow in the gap during its breakdown is revealed using an ICCD camera. Physical reasons for the observed phenomena are discussed.

**Keywords:** pulsed discharge in air and argon; steel needle electrodes; luminous tracks; micron-size particles

## 1. Introduction

At present, the breakdown of highly overvoltage gas-filled gaps continues to be intensively investigated. In the course of the research, much attention is paid to the study of nanosecond diffuse discharges in atmospheric air, formed in an inhomogeneous electric field. [1–6]. The formation of such discharges is accompanied by the generation of run-away electrons and X-rays. [1,3,6], and the discharges themselves find practical applications in various scientific and technical fields. Thus, the diffuse discharge formed in the gap with a cathode, which had a small radius of curvature, was used to clean surfaces from carbon, improve adhesion, oxidize and harden the surface of various metals [7]. The use of point cathodes makes it possible to form diffuse discharges in pressured gases in a wide range of experimental conditions [1–6]. A diffuse discharge in air at pressure <460 Torr in a gap with a positive tip using a short voltage pulse was obtained in the last century, see, for example, [8]. A diffuse discharge in atmospheric air in a gap with an anode with a small radius of curvature was first realized in [9].

When the voltage pulse duration was increased up to ≥10 ns, microchannels with an increased electron number density were evident near a cathode with a small radius of curvature on the background of a diffuse discharge, and microcraters were found on a flat anode after spark discharge and at the point of contact of the spots with the electrode surface [10-13]. It was shown in [11–13] that a large number of microdamages with a diameter from 1 to 20 μm are formed on flat metal anodes. The microdamage number and size were determined by the voltage pulse parameters and the discharge gap length. The authors of the above works found by laser interferometry, that the erosion of electrodes is associated with the appearance of microchannels in the diffuse discharge plasma. In addition, it was suggested in [10] that a decrease in the number density of particles in the microchannels due to heating. The gas heating facilitates reaching the threshold for the generation of runaway electrons and makes it possible to detect X-ray bremsstrahlung.

Microchannels in the plasma of pulsed discharges in atmospheric air in tip-plane gaps of a few millimeters long was also found in [14–16] for both voltage pulse polarities. Therewith, jets with a high concentration of ionized particles were detected near the electrodes in the case of spark breakdown. It was confirmed, see [8], those bright spots appear first on the electrode with a small radius of curvature. It was established in [15, 16] using multi-frame laser interferometry with a high temporal resolution that, in short gaps and high electric field on an electrode with a small radius of curvature, the breakdown is caused by the rapid (within 1 ns) explosive appearance of micron-sized cathode and anode spots. The spots were found to consist of highly ionized plasma with an electron number density $n_e \sim 10^{19}$–$10^{20}$ cm$^{-3}$, and spark channels of small diameter are formed from these spots. However, the stages of formation of primary streamers and a diffuse discharge with ne ≤ $10^{14}$ cm$^{-3}$ were not studied and there was no information about the observation of particle tracks in [14–16]. No registration of runaway electrons or X-rays was reported, which contribute to the formation of diffuse discharges in atmospheric air and other gases, as well.

It should be noted the studies of the initial stage of discharge in an inhomogeneous electric field were carried out in [17–19]. It was established in [17] that after the appearance of a bright spot on the cathode with a small radius of curvature, a short anode-directed spark leader is formed, the front of which moves at a low speed. Then, after a short time, bright spots appear on the flat anode, and cathode-directed spark leaders emerge from them. The front of the cathode-directed spark leaders has a high speed and reaches the front of anode-directed leaders near the cathode. After the spark leaders meet, a spark channel is formed in the gap.

The breakdown between two point electrodes in nitrogen and its mixture with water vapor was studied in [18]. Shooting with an ICCD camera showed that the breakdown begins with the formation of a streamer at the positive tip, and then a diffuse discharge is formed, which passes into a spark. A streak camera was used to study the discharge dynamics in air and nitrogen in [19]. Based on results obtained, it was stated that two stages of a streamerless spark discharge are observed at atmospheric gas pressure. The plasma radiation is dominated by the second positive and first negative nitrogen systems in the first stage with a duration of about 2 ns, while the emission of NO* molecules and the first positive nitrogen system predominates during the second stage. It can be assumed that in [19], as in [1–3,17], a diffuse discharge was formed at the first stage due to streamers, and the diffuse discharge mainly radiates on the transitions of the second positive nitrogen system [17].

Note that, in the works cited above, luminous traces of particles (tracks) were not observed in discharges at atmospheric air pressure. However, it is well known that, on the cathode of vacuum discharges, bright spots are formed, from which particles of various sizes fly apart [20]. Glowing tracks of plasma crystals were observed in a high-frequency discharge at low argon pressures in Ref. [21].

Finally, traces of luminous particles in atmospheric air discharge, formed by nanosecond voltage pulses, were discovered in recent works [22,23]. Figure 3 in [22] shows an image in which two streamers propagate from a particle in opposite directions. Straight particle tracks initiated from a tungsten wire cathode were shown in Figure 4(a) of this article at a generator voltage of 120 kV and a hydrogen pressure of 30 Torr, whereas no tracks were observed in hydrogen and other gases at atmospheric pressure. In addition, nanoparticles with sizes of ≈500 nm or less were found on the polyamide chamber wall at an air pressure of 100 Torr, see Figure 4(b) in [22].

The aim of this work is to study the discharge plasma radiation between two electrodes with a small radius of curvature in air and argon with a high spatial resolution and to confirm the appearance of thin luminous tracks.

Simultaneously, voltage and discharge current pulses were measured with a picosecond time resolution. The emission spectra and the glow of streamers and diffuse discharge, including those with spots on the electrodes, were recorded with an ICCD camera, as well.

## 2. Materials and Methods

An experimental setup similar to that described in detail in [24] is shown in Figure 1. Voltage pulses from GIN-55-01 (negative polarity) or GIN-50-1 (positive polarity) generators, the principle of operation of which is described in [25], were applied via a transmission line to electrodes located in a discharge chamber with side windows made from fused quartz.

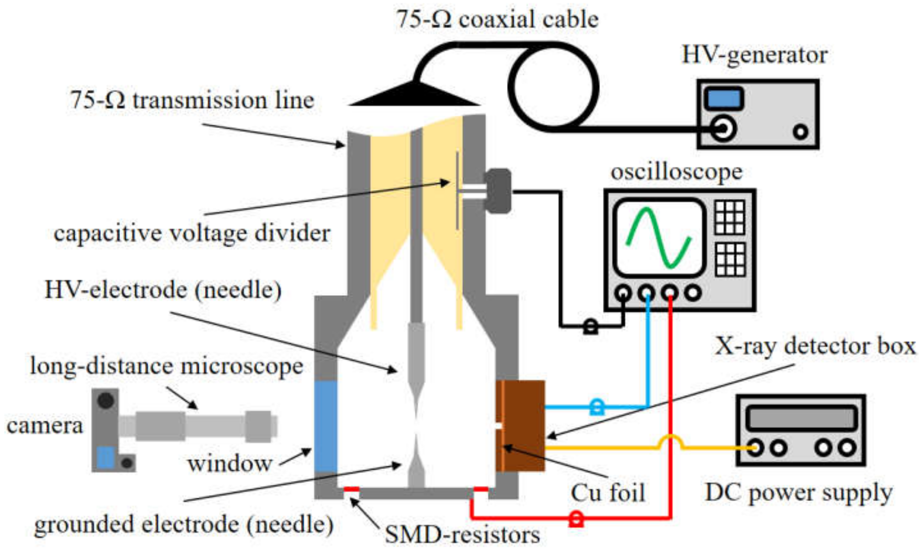


**Figure 1.** Schematic diagram of the experimental setup [25].

The GIN-55-01 generator forms voltage pulses with an amplitude in the incident wave up to -38 kV and a duration at half maximum $\tau_{0.5} \approx 0.7$ ns. Most of the results presented in this paper were obtained with the voltages pulses of -18 and -33 kV. The GIN-50-1 generator forms voltage pulses with an amplitude in the incident wave up to +25 kV and a duration at half maximum $\tau_{0.5} \approx 10$ ns. The pulse front duration was $\tau_{0.1\text{–}0.9} \approx 3$ ns. Most of the results presented in this paper were obtained with voltages pulses of +6, +11 and +16 kV. At idle, their amplitudes doubled. The presence of X-ray radiation from the discharge was measured with an HR-GaAs:Cr X-ray detector, described in [26], which was installed instead of the window after a copper foil 20 microns thick. This X-ray detector with a semiconductor sensor input window diameter of 3 mm had a high sensitivity but the pulse response was about 2 ns.

The discharge chamber was connected to the high-voltage generator by two 1-m length coaxial transmission lines (Z = 75 Ohm) and a 3-m length coaxial high-voltage cable. The transmission line near the discharge chamber had built-in capacitive voltage dividers, which were located near the discharge chamber and at a distance of 2 m from it. Such an arrangement of the dividers made it possible to measure the incident and reflected voltage waves and restore the voltage across the gap. The discharge current was measured by a current shunt with a resistance of 8.7 mΩ, assembled from thin-film SMD resistors (Vishay Intertechnology).

The large total length of the two lines made it possible to record a series of reflected voltage pulses from the discharge gap and the generator, whose resistance decreased to fractions of an ohm within ~10 ns. The reflected voltage pulses in the absence of the gap breakdown returned to it after ≈50 ns with the opposite polarity. In the case of the gap breakdown, it was possible to determine the energy deposited into the discharge plasma from measured current and voltage pulses, both in the main pulse and in reflected decayed pulses. When a diffuse discharge was formed in the gap, the impedance of the coaxial line and the plasma resistance for some time turn out to be close. This leads to efficient energy transfer to the discharge plasma, and the mode of energy input can be changed with air pressure and the generator voltage. In particular, the main part of the energy can be transferred to the discharge plasma from the first voltage pulse arriving at the gap, which greatly reduced the effect of reflected pulses on the discharge radiation characteristics.

The gap 4 mm long was formed by two needles with a base diameter of 0.75 mm. Their length after a long training was 5.5 mm, and the radii of curvature were ≈100 μm for the potential needle and ≈300 μm for the grounded one. Therewith the grounded needle during the preliminary training changed its shape over a longer length and became blunt. As a result, the radius of curvature of the transition region from the end surface of the tip with a radius of 300 μm to the surface of the cone at the tip of the needle was ≈100 μm. The training procedure with multiple pulses was used in the experiments to ensure that the shape of the needles did not change significantly from pulse to pulse. As is known, see, for example, [27], if bright spots are formed on the electrodes in a diffuse discharge, the surfaces of both electrodes are eroded. Therewith the radius of curvature of sharp needles changes significantly due to the melting of the tip after one nanosecond voltage pulse [8]. In the case of low energies per pulse and large radii of curvature of the tips, micrometer-sized craters form on their surface, but the general shape of the needles changed insignificantly [27]. In our experiments, the GIN-55-01 generator provides an energy input of 8 mJ to the matched load with a resistance of 75 Ω at a voltage pulse amplitude of 33 kV and only 3.5 mJ at 18 kV.

The signals from the capacitive voltage divider and the current shunt were fed to a Tektronix MSO64B oscilloscope (8 GHz, 20 GS/s).

The glow in the discharge gap was recorded using a Canon EOS 2000D SLR camera (number of pixels 24.7 Mp, matrix size 22.×4.9 mm, pixel size 3.72 μm) equipped with a K2 DistaMax long-distance microscope (Infinity Photo-Optical Company) with a CF-3 objective. According to the datasheet, the microscope in this configuration provided a magnification of 3.56 with a maximum resolution of 1.7 μm. The exposure duration of the camera was 1 s, and the sensitivity varied in the range of 100–3200 ISO. The spectral composition of the discharge radiation was determined using an OceanOptics HR2000 spectrometer with a known spectral sensitivity in the range of 180–1100 nm. A four-frame HSFC PRO ICCD camera was used to observe the discharge dynamics.

The chamber was evacuated with a fore-vacuum pump and filled with atmospheric air with a relative humidity of 23% or argon with purity no worse than 99.99%. Atmospheric air at pressures of 30, 100, 300 and 760 Torr and argon at pressures of 100 and 760 Torr were used in experiments

## 3. Results

### *3.1. Measurement of voltage, discharge current and X-ray radiation*

The characteristics of discharge formed in a non-uniform electric field were studied during first step. The task was to measure the features of breakdown and to determine whether runaway electrons (RAE) are generated in discharge when luminous tracks of particles with micron dimensions are evident. It was found that RAE occurs under the conditions of our experiments. This follows from the formation of the diffuse discharge at elevated pressures without an additional preionization source. Studies of the diffuse discharge formation with the measurement of the run-away electron current and X-ray radiation are performed in many works, see, for example, [10,28,29]. In our previous works [1,3,30] under similar experimental conditions runaway electrons were recorded behind a flat foil anode by a collector with a picosecond time resolution which was carried out.

In this work, it was difficult to install a collector behind the anode or near it to detect runaway electrons, therefore X-ray pulses (XR) were measured to prove RAE generation. The runaway electrons were decelerated on a grounded electrode and chamber walls and produced X-ray quanta propagating in different directions. X-rays were recorded through a side window, covered with copper foil. Voltage pulses across the gap in the idle running and in the case of gap breakdown along with the X-ray pulse are shown in Figure 2.

The X-ray pulse amplitude increased with the generator voltage increased and the gas pressure decreased, as expected. The X-ray pulse duration corresponded to the pulse response of the detector, see the data in [26]. The presence of XR, along with a diffuse discharge formation confirms the generation of runaway electrons.

Preprints (www.preprints.org) | NOT PEER-REVIEWED | Posted: 20 April 2023 doi:10.20944/preprints202304.0618.v1

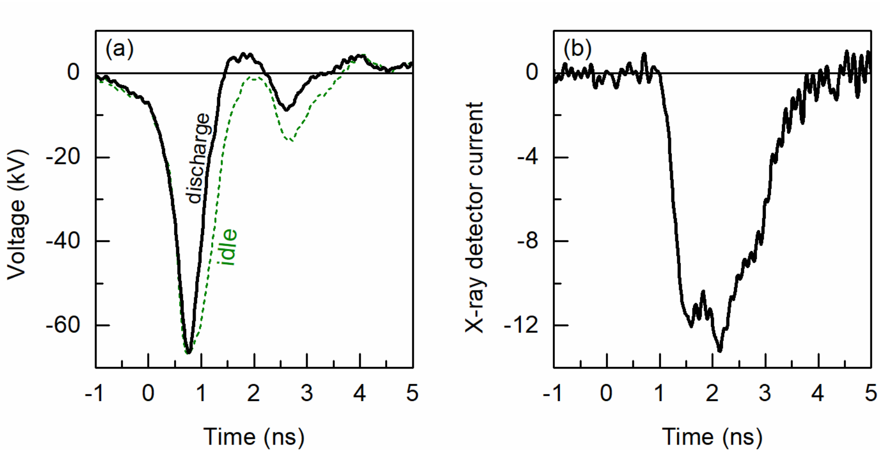


**Figure 2.** Waveforms of voltage pulses across the gap at no load operation (idle) and in the case of discharge formation (a); X-ray bremsstrahlung pulse from the side window behind 20 μm thick copper foil. Air pressure $p$=760 Torr, the voltage pulse amplitude in the incident wave is $U_0$ = 34 kV, generator GIN-55-01 (b).

RAE pulse under similar conditions in atmospheric air is much shorter and amounts to ≈100 ps [1,3]. When using the GIN-50-1 generator, due to its positive polarity and screening of the grounded cathode by the chamber walls along with the lower amplitude of the voltage pulse and its long rise time, the sensitivity of the X-ray sensor was insufficient in atmospheric air. In addition, soft X-rays were absorbed by the copper foil. However, even with the positive voltage pulses, a diffuse discharge was first formed in the gap, which then contracted with an increase in air pressure and voltage. This conclusion follows from an analysis of images, which show a diffuse discharge, and luminescence spectra in the gap. These data will be described further in Section 3.3.

The breakdown voltage depended on the gas pressure and the generator parameters. Waveforms of the voltage pulses across the gap and the discharge current in atmospheric air obtained with both generators are shown in Figure 3.

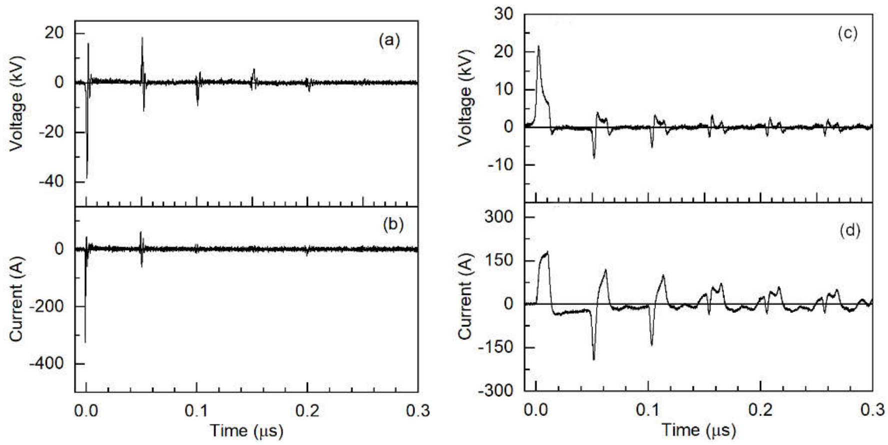


**Figure 3**. Voltage and current pulses obtained with the GIN-55-01 generator, $U_0$=-33 kV, air pressure $p$=760 Torr (a, b), and with the GIN-50-1 generator, $U_0$=+11 kV, $p$ = 100 Torr (c,d). The reflected voltage and current pulses arriving with a delay of ≈50 ns are seen after the first pulses.

With amplitude in the incident wave of -33 kV, the breakdown of gap occurred during the first voltage pulse at ≈-37 kV and was accompanied by a discharge current with an amplitude of ≈324 A (see first pulses in Figure 3a. The second voltage pulse (the first reflected one) had a complex shape. Its beginning was positive. This occurs due to the reflection of part of the pulse from the discharge gap before its breakdown and subsequent reflection from the generator, which impedance decreased to a few ohms within 10 ns. The second part of the pulse had a negative polarity, which is associated with a sub-ns breakdown time and sharp drop of the discharge plasma resistance to a value lower than the transmission line impedance. It follows from Figure 3a,b that the main electric energy is deposited into the gas-discharge load during the first voltage pulse. The second pulse of the discharge current has a low amplitude, and the third one is practically not noticeable.

When working with the GIN-50-1 generator at the voltage amplitude $U_0$=+11 kV, 22 kV in the idle mode, the gap breakdown during the first pulse occurs at air pressure not higher than 100 Torr, see Figure 3c,d. Therewith the gap breakdown occurs immediately after reaching the open circuit voltage at the beginning of the flat top of the first pulse, see Figure 3c. It is evident from the current and voltage waveforms that the main energy input into the discharge plasma was provided during the first voltage pulse. The amplitude of the reflected voltage pulses significantly decreased, but the discharge current pulses during the reflected voltage pulses had relatively large amplitude. This is explained by the discharge contraction and sharp decrease of the plasma resistance. The gap breakdown can occur during one of the reflected voltage pulses when air pressure was increased to 760 Torr and (or) the voltage amplitude $U_0$ was increased.

From the data in Figure 3, as well as from the voltage and current waveforms, obtained under different $U_0$ and $p$, it follows that the gap breakdown conditions could be changed by varying the air pressure and the generator voltage. As will be shown below, the breakdown conditions have a strong effect on the glow of the discharge plasma and the formation of the thin luminous tracks.

### *3.2. Radiation characteristics of the discharge formed by negative voltage pulses*

The most important data were obtained in our work using the long-focus microscope with a spatial resolution of 1.7 μm, which was apparently used for the first time to study the nanosecond discharge in a non-uniform electric field. Figure 4 depicts images of the interelectrode gap and the discharge glow in air at a pressure of 760 Torr and its relative humidity of 23%.

These images show that different areas can be distinguished in the discharge by their brightness, color and shape. A program for correction of the levels of brightness and contrast of the images was used for analyzing the image to show the diffuse discharge emission and highlight the thin luminous tracks (TLT) initiated by metal particles emitted from the electrodes. This was necessary because of the high brightness of white (1) and blue spots (3) observed at the electrodes. The glow of these spots dominates the original image, see Figure 4b. Spark leaders (2), which start from white bright spots, are also seen in this figure. However, in this case, the glow of the diffuse discharge and the TLT is practically not noticeable. The glow of the diffuse discharge, which occupies the whole gap, and TLT (4) become visible in the image only after correction of the luminosity and contrast levels, see Figure 4c,d. Moreover, the tracks are more noticeable in areas without a diffuse discharge; see, for example, the track in the lower left corner in Figure 4d.

Preprints (www.preprints.org) | NOT PEER-REVIEWED | Posted: 20 April 2023 doi:10.20944/preprints202304.0618.v1

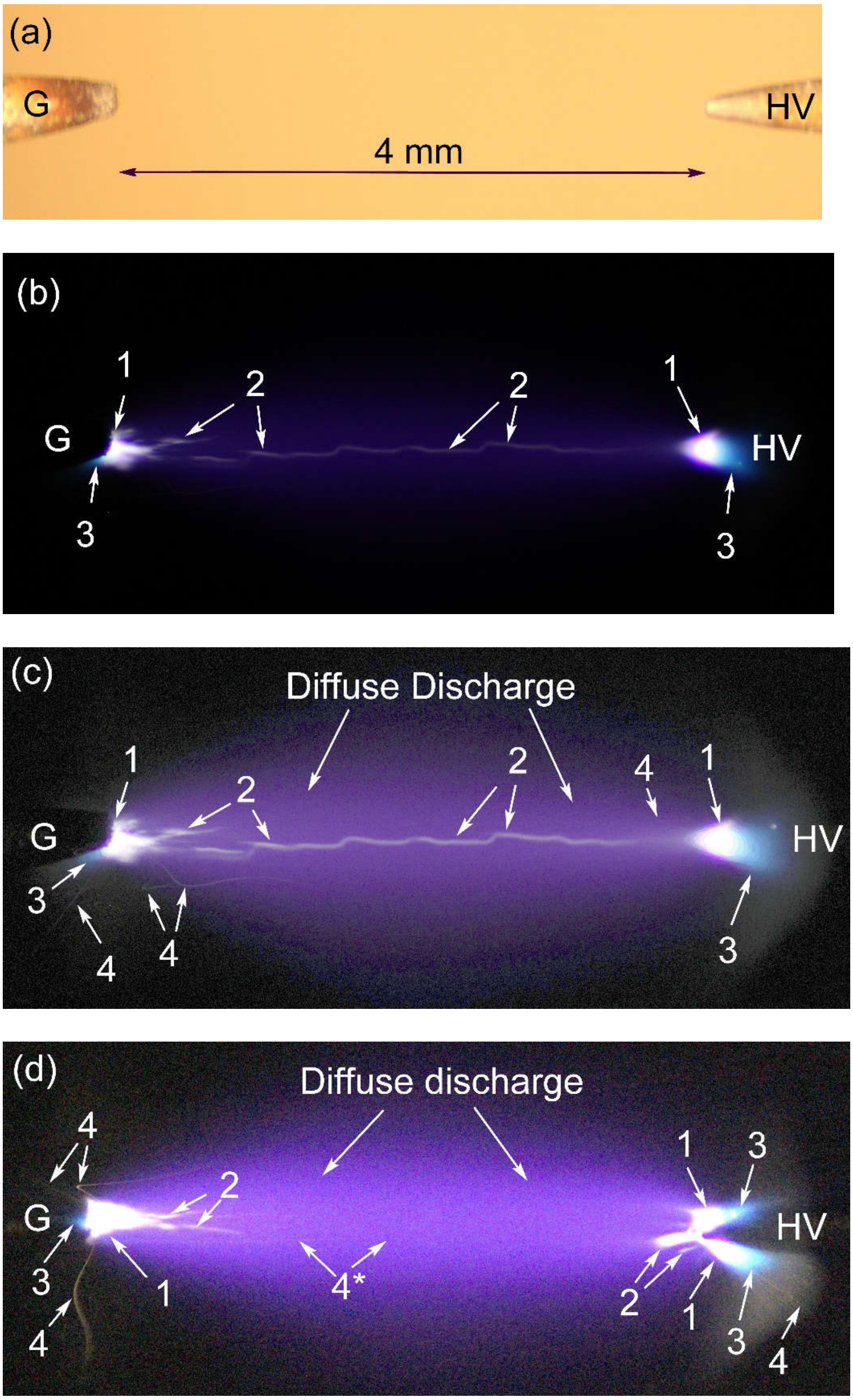


**Figure 4.** The discharge gap image, G and HV are grounded and potential electrodes (a); original image of the glow in the discharge gap (b); the same image after adjusting the brightness and contrast levels (c); image after correction of brightness and contrast levels, obtained under the same conditions as in (c), but with another voltage pulse (d); 1 – bright white spots on the electrodes on and near, 2 – spark leaders, 3 – areas of blue glow near the electrodes, 4 – thin luminous tracks with curves, 4* – straight luminous track. Air pressure $p \approx 760$ Torr, the voltage pulse amplitude in the incident wave $U_0$=-33 кВ.

The TLT color (4), as can be seen from Figure 4c,d, differs from the color of the spark leader (2), which indicates different mechanisms of their formation. The minimal track cross-section did not exceed 2 μm, which corresponds to the microscope spatial resolution. The size of the particles that lead to the formation of thin luminous tracks should be smaller. Thus, the transverse particle size on the chamber wall was ≈500 nm and less [22]. The width of the observed tracks was also affected by their position relative to the gap center. When moving away from the plane of the objective focus, tuned to the central axis of the discharge, the image was blurred and became wider.

The shape of the tracks and their length are very diverse and changed from pulse to pulse. However, TLT always adjoined the region of bright white spots on the electrodes or their periphery. TLTs could sharply reverse their direction of propagation, see Figure 4d, the region above the left electrode. Therewith several tracks can adjoin one bright spot, including those on the periphery of the white bright spot. Such a straight long track (4*) is seen in Figure 4d. Current and voltage waveforms, taken simultaneously with these images, practically did not change from pulse to pulse and were close to those shown in Figure 3(a). However, the shape and position of the white and blue spots near the electrodes, the shape and the number of spark leaders and TLCs changed from pulse to pulse. In addition, TLCs always adjoined bright white spots, which indicates the escape of particles from a part of the electrode surface, on which the bright white spots appear. For the appearance of a large number of TLC, bright white spots should be located on the tips of the electrodes. The probability of such an arrangement of bright spots increased with an increase in voltage and a decrease in air pressure.

Spectral measurements showed that with the GIN-55-01 generator in the whole pressure range (760, 300, 100, and 30 Torr), the bands of the second positive nitrogen system (2+), peak intensity on $C^3\Pi_u(v=0)\rightarrow B^3\Pi_g(v=0)$ transition at 337.1 nm, dominates in the diffuse discharge glow as it shown in Figure 5. Therewith emission of white and blue spots dominating in the visible region in the images in Figure 4, is not visible in the spectrum which shows the spectral energy density of radiation *W*. This can be associated with the low *W* value in individual lines and bands of white and blue spots compared to the UV emission on the $2^+$ system and wide spectral range of the spot emission.

### *3.3. Optical parameters of discharge radiation formed by positive voltage pulses*

Images of the discharge glow obtained with the GIN-50-1 generator, providing voltage pulses with positive polarity and duration at half maximum of ≈10 ns are shown in Figure 6. Changing voltage pulse parameters affected the characteristics of the discharge. Diffuse discharge without spark channel was seen in the corrected images only at low voltage amplitude in the incident wave (not higher +6 kV) and air pressures of 30 and 100 Torr, see Figure 6a. Therewith, both curved tracks with a change in the direction of motion to the opposite (4) and straight tracks (4*) were evident. Spark leaders (2) and blue glow regions (3) were also formed, but the discharge constriction did not occur.

Formation of a wide spark channel was seen in the gap when $U_0$ and air pressure were increased to +11 kV and 100 Torr, respectively, see Figure 6b. The discharge constriction is confirmed with the current and voltage waveforms, shown in Figure 3(b), which indicate a sharp decrease in the discharge plasma resistance. Note that, particle tracks were also recorded in atmospheric air, but the probability of their appearance decreases with the GIN-50-1 generator.

Preprints (www.preprints.org) | NOT PEER-REVIEWED | Posted: 20 April 2023 doi:10.20944/preprints202304.0618.v1

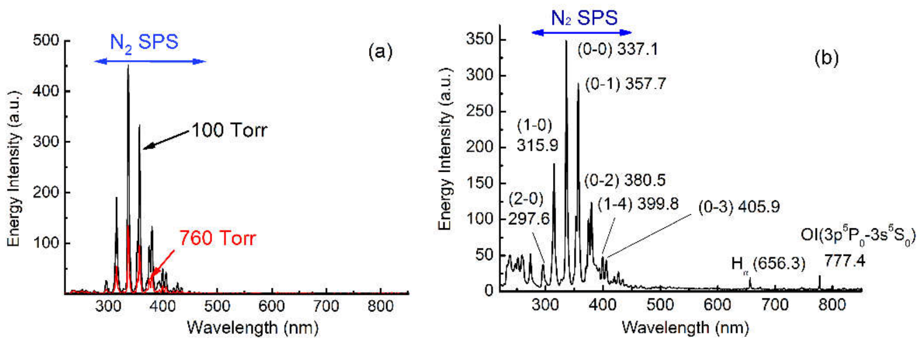


**Figure 5.** Emission spectra of the discharge plasma obtained with the GIN-55-1 generator, $U_0$=-33 kV (a) and GIN-50-1 generator, $U_0$=+6 kV (b). The pulse repetition rate is 10 Hz. ($v_i$)-($v_j$) denotes transitions of nitrogen 2$^+$ system in nm.

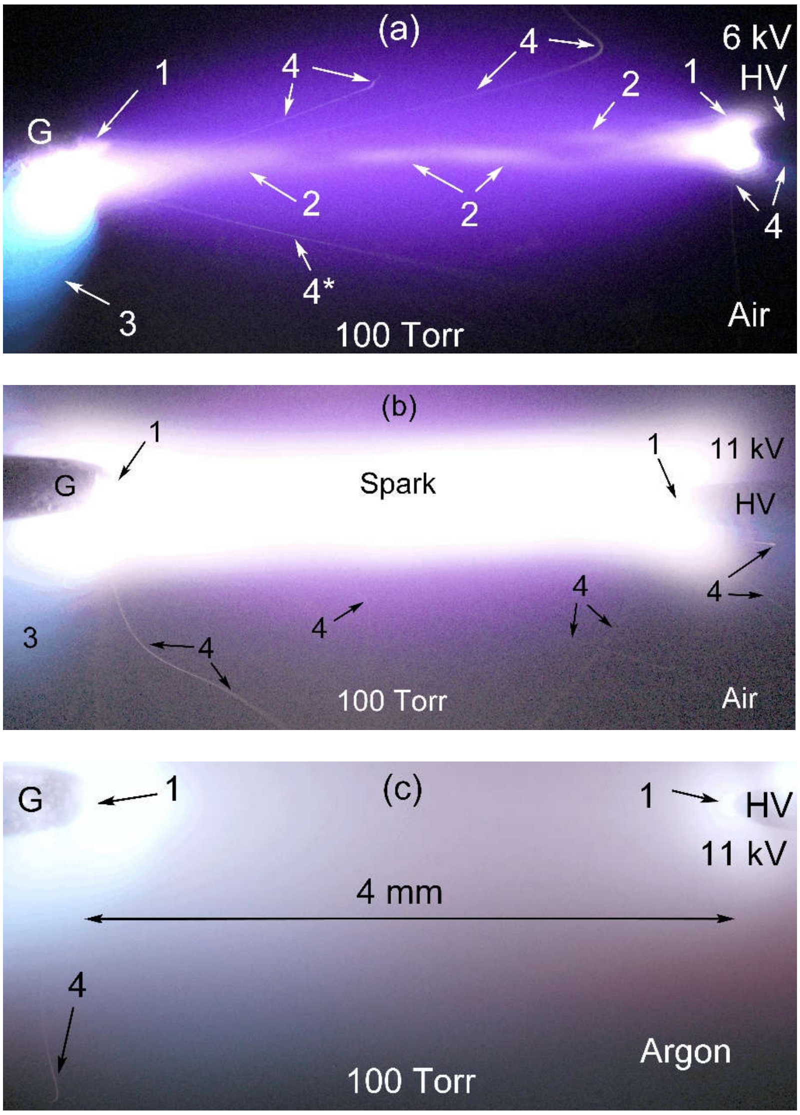


**Figure 6.** Images of the discharge after correction of the brightness and contrast levels, obtained in air (a,b) and argon (c) at *p*=100 Torr for different amplitudes of the voltage +$U_0$ in the incident wave from the GIN-50-1 generator. G and HV designate grounded potential electrodes. 1 – bright white spots on the electrodes near the tips, 2 – spark leaders, 3 – glowing blue area near the electrodes, 4 – thin luminous tracks with curves, 4* – straight track.

Preprints (www.preprints.org) | NOT PEER-REVIEWED | Posted: 20 April 2023 doi:10.20944/preprints202304.0618.v1

Recording the spectra at different pressures (760, 100, and 30 Torr) with the GIN-50-1 generator showed that bands of the second positive nitrogen system dominate in discharge glow only at $p = 30$ Torr and $U_0 = 6$ kV, see. Figure 5(b). However, even under these conditions, visible and UV broadband radiation appears in the spectra. The intensity and bandwidth of this radiation increase with air pressure and amplitude of the voltage pulse. The broadband radiation with wavelengths <280 nm, as was established earlier in [17], is emitted from bright white spots on the electrodes, spark leaders, the spark channel and observed in different gases (He, $H_2$, CO, Xe, $CO_2$). The total radiation energy density $W$ from discharge in atmospheric air exceeds the most intense band of $2^+$ nitrogen system at 337.1 nm. The number of registered TLTs decreases, as well.

TLTs were observed when air was replaced with argon, Figure 6(c). However, the number of TLTs in a single pulse and the number of pulses in which thin luminous tracks were observed decreased. From the comparison of Figure 6(b,c), it follows that only one track is visible in argon, which is adjacent to the grounded electrode of negative polarity, ceteris paribus. The number of TLTs in air is an order of magnitude greater, and the tracks originate from bright white spots on both electrodes, Figure 6(b).

## 4. Discussion

From the analysis of the images, the number of which was more than 150, the following conclusions can be made.

1. TLTs are formed mainly from the part of the electrode surface with bright white spots appearing. The shape and number of the tracks vary from pulse to pulse and depend on the gas type and pressure, the voltage pulse amplitude.

2. A decrease in the amplitude of the voltage pulse from the GIN-55-01 generator usually reduces the length of the TLTs, and their number. As, the number of visible TLTs decreases with the gas pressure, while their apparent length shortens. At a pressure of 30 Torr, short TLTs were observed only at $U_0$=-18 kV. A decrease in the amplitude of the voltage pulse from the GIN-55-01 generator usually shortens the length of the TLTs and reduces their number. The number of visible TLTs also becomes smaller and their apparent length shortens at low gas pressure. At a pressure of 30 Torr and $U_0$=-18 kV, only short TLTs were observed.

3. TLT can change the direction of movement and move in the opposite direction.

4. TLT can be connected to both high-voltage and grounded electrodes.

5. Discharge constriction does not limit the appearance of TLTs.

6. Studies of the formation of streamers and diffuse discharge with the ICCD camera showed that TLTs are not observed on the background of streamers forming diffuse discharge and on the background of the diffuse discharge with bright spots on the electrodes.

The formation of TLTs can be explained in the following way. The observed tracks are traces of hot metal particles that fly out of the electrode surface in the area of its contact with the dense plasma. Therefore, the TLT color differs from the color of the spark leaders. Initial plasma is created due to heating and thermal explosion of micro-inhomogeneities through which a current with a high density flows [27]. As was shown in [31–34], a decrease in the breakdown voltage in a vacuum cannot be associated only with explosive electron emission from the cathode. Various phenomena must be considered to understand the limitations of the electrical strength of vacuum insulation. Thus, the calculations made in [34] show that the cathode material is subjected to destructive mechanical stresses in an unheated region, the size of which significantly exceeds the size of the explosive electron emission center. As a result, the appearance of a primary cathode spot during vacuum breakdown and the plasma formation near the electrode surface result in multiple local destructions on the periphery of the electrode surface under the action of mechanical stresses.

In our conditions as the spot sizes increased, some of the spots initiated TLTs. Moreover, the tracks were observed from the electrode surface with both voltage pulse polarities. The visible luminescence of TLTs is explained by their comparatively high temperature. The sharp curves of the tracks and the change of direction of their movement can be explained by a change in the polarity and magnitude of the TSC charge along with the change of the voltage polarity across the gap

 doi:10.20944/preprints202304.0618.v1

reflected pulses. It has been established that TSTs during one voltage pulse are adjacent to both electrodes. There are pulses in which a large number of TLTs are in contact with one bright spot, and some of TLTs are in contact with the electrode at the periphery of the bright spots. It can be assumed that the appearance of TSCs in our experiments is associated with an increase in the electric field near electrodes with a small radius of curvature, and the appearance of a dense plasma near the electrodes as in vacuum discharges, see [31–34]. This leads to the departure of micro- and nanoparticles of metal from the electrode surface under the influence of mechanical stresses.

High voltage pulses with short rise time can increase mechanical stresses. Apparently, this is not enough. Additional amplification of the electric field is necessary, and the explosion of microprotrusions on the electrodes due to the formation of plasma (white bright spots) can provide field enhancement. The formation of bright spots on the electrodes was discussed in [34].

It can also be assumed that nanoparticles increase the electric field in the region of their appearance and at a distance from the electrodes. This can lead to the formation of thin streamers with high electron number density.

## 5. Conclusion.

The plasma of nanosecond discharges formed in an inhomogeneous electric field was studied with a high spatial resolution using a long-distance microscope. Thin luminous tracks with a minimum transverse size of lower 2 μm were found against the background of diffuse discharge in air and argon between the electrodes, as well as on the side of the electrodes. It has been established that TLTs are usually adjacent to bright spots on the electrodes, have a variety of shapes, and can change the direction of their movement to the opposite. Their length in atmospheric air can reach the length of the discharge gap.

We assume that the TLT formation is associated with the escape of metal particles from the surface of the electrodes under the influence of stresses that arise due to mechanical phenomena. In this case, the amplification of the electric field due to the shape of the electrodes and the formation of a dense plasma via a thermal explosion of microprotrusions affect the TLT occurrence. A similar phenomenon is observed in vacuum discharges due to explosive electron emission [31–34]. TLTs in diffuse discharges in air, argon and, apparently, in other gases, are in contact with both electrodes in contrast to the vacuum discharges

The tracks differ in color from the spark leaders, which lead to the formation of spark channels in diffuse discharges. In addition, the metal particles, escaping from electrodes, can enhance the electric field in the region of their appearance during voltage pulses and initiate the development of streamers and then along their path. The trajectories of TLTs and streamers should coincide in separate sections of their path and be straight, which was recorded in many pulses, see Figure 4(b).

**Funding:** This research was supported by the Ministry of Science and Higher Education of the Russian Federation within Agreement no. 075-15-2021-1026 of 15 November 2021.

**Author Contributions:** Conceptualization, writing original draft, V.T.; experiments, analysis, methodology, D.B. and P.A.; editing, project administration, D.S. All authors have read and agreed to the published version of the manuscript.

**Data Availability Statement:** Data are contained within the paper.

**Conflicts of Interest:** The authors declare no conflict of interest. The funders had no role in the design of the study; in the collection, analyses, or interpretation of data; in the writing of the manuscript, or in the decision to publish the results.

## References

1. Tarasenko, V.F.; Baksht, E.K.; Burachenko, A.G.; Kostyrya, I.D.; Lomaev, M.I.; Rybka, D.V. Generation of Supershort Avalanche Electron Beams and Formation of Diffuse Discharges in Different Gases at High Pressure. Plasma Devices and Operations **2008**, 16, 267–298. DOI: 10.1080/10519990802478847

2. Chng, T.L.; Brisset, A.; Jeanney, P.; Starikovskaia, S.M.; Adamovich, I.V.; Tardiveau, P. Electric Field Evolution in a Diffuse Ionization Wave Nanosecond Pulse Discharge in Atmospheric Pressure Air. Plasma Sources Sci. Technol. **2019**, 28, 09LT02. https://doi.org/10.1088/1361-6595/ab3cfc
3. Tarasenko, V. Runaway Electrons in Diffuse Gas Discharges. Plasma Sources Sci. Technol. **2020**, 29, 034001. https://doi.org/10.1088/1361-6595/ab5c57
4. Černák, M.; Hoder, T.; Bonaventura, Z. Streamer Breakdown: Cathode Spot Formation, Trichel Pulses and Cathode-sheath Instabilities. Plasma Sources Sci. Technol. **2019**, 29, 013001. https://doi.org/10.1088/1361-6595/ab5051
5. Brisset, A. ; Tardiveau, P. ; Gazeli, K. ; Bournonville, B. ; Jeanney, P. ; Ouaras, K. ; Magne, L.; Pasquiers, S. Experimental Study of the Effect of Water Vapor on Dynamics of a High Electric Field Non-equilibrium Diffuse Discharge in Air. J. Phys. D. **2021**, 54, 215204. **DOI** 10.1088/1361-6463/abe81e
6. Huang, B.; Zhang, C.; Ren, C.; Shao, T. Guiding Effect of Runaway Electrons in Atmospheric Pressure Nanosecond Pulsed Discharge: Mode Transition from Diffuse Discharge to Streamer. Plasma Sources Sci. Technol. **2022**, 31, 114002. https://doi.org/10.1088/1361-6595/ac9c2c
7. Erofeev, M.; Lomaev, M.; Ripenko, V.; Shulepov, M.; Sorokin, D.; Tarasenko, V. Generators of Atmospheric Pressure Diffuse Discharge Plasma and Their Use for Surface Modification. Plasma **2019**, 2, 27–38. https://doi.org/10.3390/plasma2010004
8. Korolev, Iu. D.; Kuzmin, V.A.; Mesiats, G.A. Nanosecond Gas Discharge in an Inhomogeneous Field with Explosive Processes on the Electrodes. Soviet Physics Technical Physics **1980**, 25, 418–420. Bibcode: 1980SPTP...25..418K
9. Kostyrya, I.D.; ;Tarasenko, V.F.. Formation of a Volume Discharge in Air at Atmospheric Pressure upon Application of Nanosecond High-voltage Pulses. Russian physics journal **2004**, 47, 1314–1316. DOI: https://doi.org/10.1007/s11182-005-0074-5
10. Rep'ev, A.G.; Repin, P.B.; Pokrovskiĭ, V.S. Microstructure of the Current Channel of an Atmospheric-Pressure Diffuse Discharge in a Rod-Plane Air Gap. Tech. Phys. **2007**, 52, 52–58. https://doi.org/10.1134/S1063784207010094
11. Almazova, K.I.; Belonogov, A.N.; Borovkov, V.V.; Kurbanismailov, V.S.; Khalikova, Z.R.; Omarova, P.K.; Ragimkhanov, G.B.; Tereshonok, D.V.; Trenkin, A.A. Investigation of the Microchannel Structure in the Initial Phase of the Discharge in Air at Atmospheric Pressure in the "Pin (anode)-Plane" Gap. Phys. Plasmas **2020**, 27, 123507. https://doi.org/10.1063/5.0026192
12. Almazova, K.I.; Belonogov, A.N.; Borovkov, V.V.; Khalikova, Z.R.; Ragimkhanov, G.B.; Tereshonok, D.; Trenkin, A.A. Investigation of Plasma Properties in the Phase of the Radial Expansion of Spark Channel in the Pin-to-Plate Geometry. Plasma Sources Sci. Technol. **2021**, 30, 095020. https://doi.org/10.1088/1361-6595/aba8cc
13. Almazova, K.I.; Belonogov, A.N.; Borovkov, V.V.; Kurbanismailov, V.S.; Ragimkhanov, G.B.; Tren'kin, A.A.; Tereshonok, D.V.; Khalikova, Z.R. Plasma and Gas-Dynamic Near-Electrode Processes in the Initial Phase of a Microstructured Spark Discharge in Air. Tech. Phys. Lett. **2020**, 46, 737–740. https://doi.org/10.1134/S1063785020080039.
14. Parkevich, E.V.; Ivanenkov, G.V.; Medvedev, M.A.; Khirianova, A.I.; Selyukov, A.S.; Agafonov, A.V.; Mingaleev, A.R.; Shelkovenko, T.A.; Pikuz, S.A. Mechanisms Responsible for the Initiation of a Fast Breakdown in an Atmospheric Discharge. Plasma Sources Sci. Technol. **2018**, 27, 11LT01. https://doi.org/10.1088/1361-6595/aaebdb
15. Parkevich, E.V.; Medvedev, M.A.; Khirianova, A.I.; Ivanenkov, G.V.; Selyukov, A.S.; Agafonov, A.V.; Shpakov, K.V.; Oginov, A.V. Extremely Fast Formation of Anode Spots in an Atmospheric Discharge Points to a Fundamental Ultrafast Breakdown Mechanism. Plasma Sources Sci. Technol. **2019**, 28, 125007. https://doi.org/10.1088/1361-6595/ab518e
16. Smaznova, K.; Khirianova, A.; Parkevich, E.; Medvedev, M.; Varaksina, E.; Khirianov, T.; Oginov, A.; Selyukov, A. Precise Optical Registration of Fine-structured Electrical Sparks and Related Challenges. Opt. Express **2021**, 29, 35806–35819. https://doi.org/10.1364/oe.431837
17. Shao, T.; Tarasenko, V.F.; Zhang, C.; Lomaev, M.I.; Sorokin, D.A.; Yan, P.; Kozyrev, A.V.; Baksht, E.K. Spark Discharge Formation in an Inhomogeneous Electric Field under Conditions of Runaway Electron Generation. J. Appl. Phys. **2012**, 111, 023304. https://doi.org/10.1063/1.3677951
18. Van der Horst, R.M.; Verreycken, T.; Van Veldhuizen, E.M.; Bruggeman, P.J. Time-resolved Optical Emission Spectroscopy of Nanosecond Pulsed Discharges in Atmospheric-pressure N2 and N2/H2O Mixtures. J. Phys. D. **2012**, 45, 345201. https://doi.org/10.1088/0022-3727/45/34/345201
19. Patel, K.; Saha, A.; Zhou, T.; Meyer, T.R.; Bane, S.; Satija, A. Spectrally Filtered ps–ns Emission Dynamics of Atmospheric-pressure Nanosecond Pulsed Plasmas. Appl. Phys. Lett. **2022**, 120, 014101. https://doi.org/10.1063/5.0073630.
20. Beilis, I. Plasma and Spot Phenomena in Electrical Arcs, Springer Series on Atomic, Optical, and Plasma Physics, Springer Cham, **2020**; Vol. 113. pp. 255–283. https://doi.org/10.1007/978-3-030-44747-2

21. Syrovatka R.A.; Lipaev A.M.; Naumkin V.N.; Klumov B.A. Plasma Crystal in (3+1) Dimensions. JETP Letters. **2022**, 116, 869–834. DOI: https://doi.org/10.1134/S0021364022602676
22. Tarasenko, V.; Vinogradov, N.; Beloplotov, D.; Burachenko, A.; Lomaev, M.; Sorokin, D. Influence of Nanoparticles and Metal Vapors on the Color of Laboratory and Atmospheric Discharges. Nanomaterials **2022**, 12, 652. https://doi.org/10.3390/nano12040652
23. Lomaev, M., Tarasenko, V., Shulepov, M., Beloplotov, D. and Sorokin, D., Nano-and Microparticles of Carbon as a Tool for Determining the Uniformity of a Diffuse Discharge Exposure. Surfaces, **2023**, 6, 40–52. https://doi.org/10.3390/surfaces6010004
24. Panchenko, A.N.; Beloplotov, D.V.; Kozevnikov, V.V.; Sorokin, D.A.; Tarasenko, V.F.. Wide Emission Bands of Plasma of a Sub-Nanosecond Discharge in Xenon and Inaccuracies in Their Measurements. IEEE Trans. Plasma Sci. **2021**, 49, 1614–1620. **DOI:** 10.1109/TPS.2021.3070333
25. Efanov, V.M.; Efanov. M.V.; Komashko, A.V.; Kriklenko, A.V., Yarin, P.M.; Zazoulin S.V. Ultra-wideband, short pulse electromagnetics 9, Springer-Verlag, New York, **2010**, pp.301–305. https://doi.org/10.1007/978-0-387-77845-7
26. Chsherbakov, I.; Chsherbakov, P.; Lozinskaya, A.; Mihaylov, T.; Novikov, V.; Shemeryankina, A.; Tolbanov, O.; Tyazhev, A.; Zarubin, A.; Beloplotov, D.; Tarasenko, V. Response of HR-GaAs: Cr Sensors to Subnanosecond X-and β-ray Pulses. J. Instrument. **2019**, 14, C12016. DOI 10.1088/1748-0221/14/12/C12016
27. Korolev Y.D.; and Mesyats G. A. Field-Emission and Explosive Processes in Gas Discharges, Novosibirsk, Nauka, **1982**; 255 p. [in Russian].
28. Tarasova, L.V.; Khudyakova, L N, Loiko, T.V.; Tsukerman V.A. Fast Electrons and X-ray from Nanosecond Gas Discharges at Pressures 0.1–760 Torr. Soviet Physics Technical Physics. **1974**, 19, 351–355. Bibcode: 1974SPTP...19..351T
29. Babich, LP. High-energy Phenomena in Electric Discharges in Dense Gases: Theory, Experiment, and Natural Phenomena, Futurepast Incorporated, Arlington Va, ISTC science and technology series, **2003**; vol. 2, 358 p.
30. Beloplotov, D.V.; Genin, D.E.; Pechenitsin, D.S. The Polarity Effect of Nanosecond Voltage Pulses on the Propagation of Streamers in a Point-to-Plane Gap Filled with Air. Jap. J. Appl. Phys. **2020**, 59, SHHC06. https://doi.org/10.35848/1347-4065/ab70a9
31. Nefedtsev, E.V.; Onischenko, S.A. 2021, Position of Erosion Marks on the Surface of Single-Crystal and Coarse-Grained Cathodes after a Short-Pulse Vacuum Spark. 29th International Symposium on Discharges and Electrical Insulation in Vacuum (ISDEIV), Padova, Italy Sep 26–30, **2021**; pp.23–26. **DOI:** 10.1109/ISDEIV46977.2021.9586987
32. Yakovlev, E.V.; Petrov, V.I.; Onischenko, S.A.; Nefedtsev, E.V. **2021**, September. Short-pulse breakdown of near-cathode sheath in the presence of a local magnetic field. 29th International Symposium on Discharges and Electrical Insulation in Vacuum (ISDEIV), Padova, Italy, Sept. 26–30, **2021**; pp.81–84. **DOI:** 10.1109/ISDEIV46977.2021.9586962
33. Korsbäck, A.; Djurabekova, F.; Wuensch, W. Statistics of Vacuum Electrical Breakdown Clustering and the Induction of Follow-up Breakdowns. AIP Advances. **2022**, 12, 115317. https://doi.org/10.1063/5.0111677
34. Nefedtsev, E.V.; Onischenko, S.A. Modification of the Cathode Material around the Explosive Electron Emission Centers in the Spark Stage of Vacuum Breakdown. Tech. Phys. Lett. **2022**, 48, 69–71. DOI: 10.21883/PJTF.2022.22.53804.19307